JOINT EUROPEAN TORUS JET

JET-P(89)46

B. Balet, V.P. Bhatnagar, J.G. Cordey, G.W. Hammett, T. Hellsten, M. Keilhacker, S.L. Milora, P.D. Morgan, C. Sack, G.L. Schmidt, A. Taroni, P.R. Thomas, K. Thomsen, F. Tibone, M. von HeUermann, M.L. Watkins and H. Weisen

Confinement Properties of JET Plasmas with Different Temperature and Density Profiles

Confinement Properties of JET Plasmas with Different Temperature and Density Profiles

B. Balet, V.P. Bhatnagar, J.G. Cordey, G.W. Hammett, T. Hellsten, M. Keilhacker, S.L. Milora, P.D. Morgan, C. Sack, G.L. Schmidt, A. Taroni, P.R. Thomas, K. Thomsen, F. Tibone, M. von HeUermann, M.L. Watkins and H. Weisen

JET Joint Undertaking, Culham Science Centre, OX14 3DB, Abingdon, UK

Preprint of a paper to be published in
Plasma Physics and Controlled Fusion

CONFINEMENT PROPERTIES OF JET PLASMAS WITH DIFFERENT TEMPERATURE AND DENSITY PROFILES

M. L. Watkins, B. Balet, V. P. Bhatnagar, J. G. Cordey, G. W. Hammett, T. Hellsten, M. Keilhacker, S. L. Milora, P. D. Morgan, C. Sack, G. L. Schmidt, A. Taroni, P. R. Thomas, K. Thomsen, F. Tibone, M. von Hellermann, H. Weisen
and
the JET Team[1]

JET Joint Undertaking, Abingdon, Oxon., OX14 3EA, UK

ABSTRACT

The confinement properties of plasmas with substantially different temperature and density profiles have been analysed. The effects of fast particles and energy pedestals on the overall confinement of plasma energy in limiter (L-mode) and X-point (L- and H-modes) discharges heated by NBI or ICRF or both are determined. The importance of the bootstrap current when such energy pedestals are formed is noted. Using sets of consistent experimental data, including ion temperature profile measurements, the local transport properties are compared in the L- and H-phases of a single null X-point medium density NBI heated discharge, the "enhanced" confinement phase of a limiter high density pellet-fuelled and ICRF heated discharge, the hot-ion phase of a double null X-point low density NBI heated discharge and the hot-ion and H-phases of a double null X-point low density high temperature NBI heated discharge.

KEYWORDS

Confinement; H-mode; hot-ion mode; interpretation; JET; pellet; plasma; tokamak; transport.

INTRODUCTION

The flexibility of the JET apparatus and its systems has allowed plasmas with substantially different temperature and density profiles (Bickerton and the JET Team, 1989). In a single null X-point configuration deuterium neutral beam injection (NBI) at 80kV has been used to heat medium/high density plasmas; very flat, and even hollow, density profiles develop during the H-phase (Keilhacker and the JET Team, 1989). In a double null X-point configuration lower density, higher temperature H-mode discharges have been achieved with NBI alone (Balet *et al.*, 1989) and in combination with ion cyclotron resonance heating (ICRH) (Tubbing *et al.*, 1989); these tend to have mildly peaked density profiles. In such a configuration NBI has also heated low density plasmas with highly peaked temperature and density profiles, reminiscent of the TFTR "supershot" regime (Strachan *et al.*, 1987). The central ion temperature, $T_i(0)$, reaches 23keV with a central electron temperature, $T_e(0) \sim 8$keV and a central electron density, $n_e(0) \sim 2.10^{19} m^{-3}$ (Thomas and the JET Team, 1989; Tibone *et al.*, 1989). In a limiter configuration ICRH has been used to obtain hot electron plasmas with $T_e(0)$ up to 12keV and $T_i(0) \sim 7$keV at $n_e(0) \sim 3.5 10^{19} m^{-3}$ (Start *et al.*, 1989). In combination with the injection of deuterium pellets very peaked density and temperature profiles have been obtained with $n_e \sim 10^{20} m^{-3}$,

For a list of the JET Team members, see Lomas and the JET Team, 1989.

$T_e \sim 10$keV and $T_i \sim 8$keV (Schmidt and the JET Team, 1989). Using NBI and ICRH together, high $T_i(0)$ and $T_e(0)$ have been obtained simultaneously.

In this paper, the confinement of a number of these different types of discharges are discussed. Firstly, the overall confinement properties are compared. Particular emphasis is placed on identifying the contribution of fast ions (Thomas and the JET Team, 1989) and energy pedestals (Keilhacker and the JET Team, 1989; Thomsen *et al.*, 1989) to the confinement of the bulk plasma. The importance of the bootstrap current (Cordey *et al.*, 1988; Stubberfield *et al.*, 1989) and its effect on the stability of ballooning modes (O' Brien *et al.*, 1989) when such energy pedestals form is also noted.

Secondly, the JET experimental data and the interpretive and predictive methods used to describe the local transport properties of the bulk plasma are summarised. A substantial diagnostic capability is complemented by a suite of analysis codes, which includes the time dependent energy balance code, TRANSP (Hawryluk, 1980; Goldston *et al.*, 1981), the timeslice energy balance code, FALCON (Tibone *et al.*, 1989) and the predictive transport code, JETTO (Taroni *et al.*, 1989).

Thirdly, these methods are applied to consistent sets of data for four specific discharges that exhibit the extremes of profiles and the best confinement properties observed in JET. These studies comprise: a 3MA/3.1T single null X-point, medium density, H-mode discharge heated by 8MW of NBI; a 3MA/3T limiter discharge of high density, pellet-fuelled and ICRF heated; a 3MA/3.4T double null X-point, low density, hot ion discharge heated with 21MW of NBI; and a 3MA/3.4T double null X-point, low density, high temperature H-mode discharge heated by 10.5MW of NBI.

GLOBAL CONFINEMENT PROPERTIES

For limiter (L-mode) discharges Thomas and the JET Team (1989) pointed out that the overall confinement of plasma energy is apparently insensitive to variations in the central temperature, or density, by a factor two. This is shown in Fig. 1(a) for a data set comprising discharges at 3MA/2.8-3.4T and distinguished according to whether $T_e(0)$, $T_i(0)$, $T_e(0)$ and $T_i(0)$ or $n_e(0)$ is high (Fig. 1(b)). This result does not preclude the possibility of better central confinement, where the temperatures and densities are high, but, for these discharges, the central volume is relatively small and contributes little to the average temperature or density. In fact, even when pellets are injected deep into an ohmic plasma and subsequently heated by ICRF, the density and temperature profiles remain very peaked, but, during a phase of "enhanced" confinement, the overall confinement is only some 20% better than after this phase (Milora *et al.*, 1989).

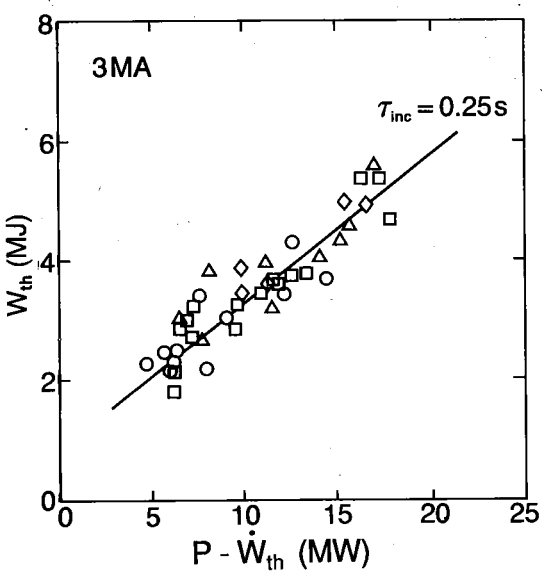

Fig. 1(a). Total plasma energy, W_{th}, as a function of net input power for 3MA JET limiter discharges.

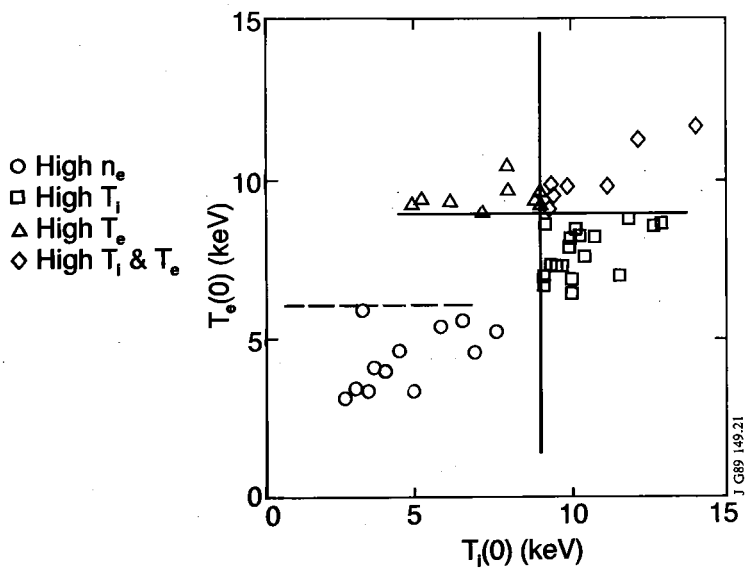

Fig. 1(b). Characterisation of the 3MA JET limiter discharges according to $T_e(0)$ and $T_i(0)$.

The L-mode data of Fig. 1(a) have been characterised by an off-set linear scaling law for the total plasma energy, W_{th}:

$$W_{th} = W_{os} + \tau_{inc} (P - dW_{th}/dt) \quad (1)$$

where $\tau_{inc} = 0.25$s is the incremental confinement time (Callen *et al.*, 1987).

In the single null X-point configuration at the same plasma current, the overall energy confinement is somewhat better during the L-phase (Tanga and the JET Team, 1987). In the H-phase, however, the density and temperature profiles are broader and the confinement is better by a factor of 2. This is shown by the diamagnetic measurement of the stored energy, W, as a function of net input power for a dataset of 3MA/2.8T single null X-point discharges (Fig. 2).

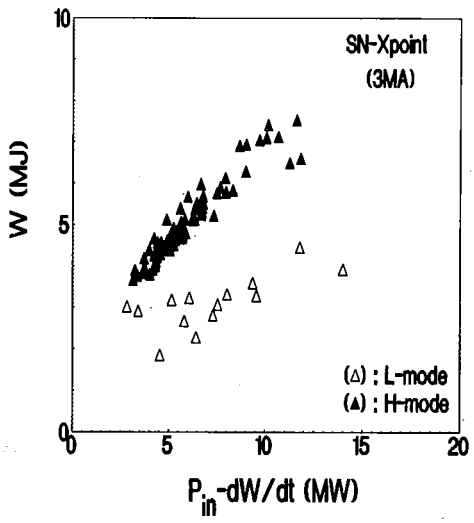

Fig. 2. Total stored energy, W, as a function of net input power for 3MA JET single null X-point discharges in L- and H-modes.

Much of the improvement in the overall energy confinement in the H-phase can be attributed to the development of pedestals in energy, as seen by the LIDAR Thomson scattering system in the steep edge gradients in the electron density, and sometimes the electron temperature also (Fig. 3). The contribution of these pedestals to the overall energy confinement must be extracted before the intrinsic confinement of the bulk plasma can be established (Keilhacker and the JET Team, 1989; Thomsen *et al.*, 1989).

Consider the simplified total energy balance equation:

$$3\, d(nT)/dt = -\nabla.Q + p \quad (2)$$

p is the net heating rate and the total heat flux, Q, is assumed to comprise a diffusive term proportional to the temperature gradient, ∇T, and a negative, non-diffusive flow term which could be a heat pinch (Callen *et al.*, 1987) or a critical electron temperature gradient (Rebut, Lallia and Watkins, 1989).

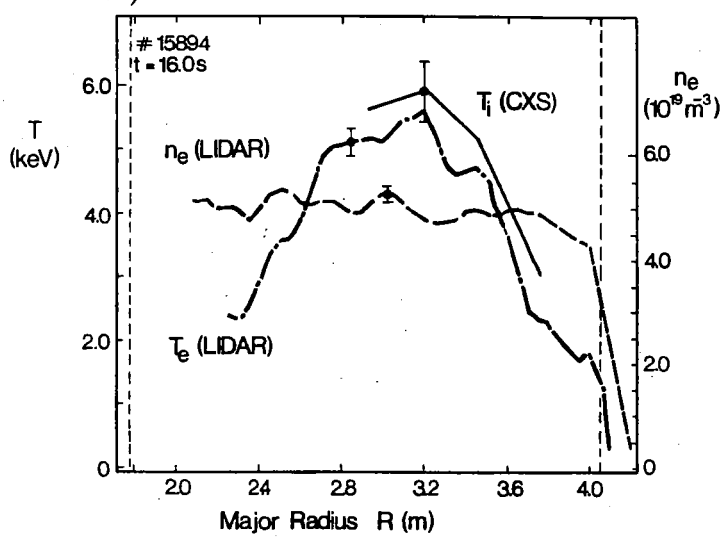

Fig. 3. Radial profiles of electron density, n_e, electron temperature, T_e, and ion temperature, T_i, during the H-phase of a 3MA JET single null X-point discharge. The dashed line indicates the radius of the 95% flux surface.

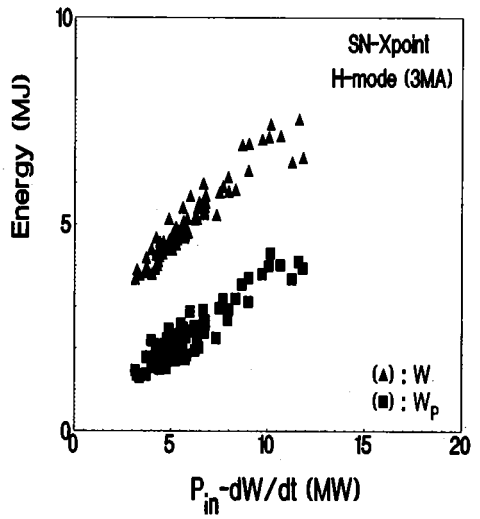

Fig. 4. Total stored energy, W, and the pedestal energy, W_p (evaluated at the radius of the 95% flux surface), as a function of net input power during the H-phase of a 3MA JET single null X-point discharges.

Integrating eq. (2) three times gives an equation for the total stored energy, $W_{th} = \int nT dV$:

$$W_{th} = W_p + W_o + \tau_\chi \{\eta_Q P_{in} - \eta_{nT} (dW_{th}/dt)\} \quad (3)$$

The pedestal energy, W_p, appears naturally in this formulation, as does the usual off-set term, W_0. The "ideal" incremental confinement time, τ_χ, depends on the radial profile of the thermal diffusivity, χ, as do the heating effectiveness parameters, η_Q and η_{nT}. The pedestal energies, evaluated at the radius of the 95% flux surface during the H-phase of 3MA single null X-point discharges are plotted in Fig. 4 against the net input power. A pedestal energy of up to 4MJ contributes substantially to the total stored energy. Furthermore, there is no pronounced degradation of W_p with input power. The values of W_p obtained in the L-phases which precede the H-phases are scattered in a range up to 1MJ and also apparently show no degradation with input power. The energy differences, $W-W_p$, for the H- and L-phases of the discharges are similar. However, to compare in detail the confinement properties of the bulk plasma in the L- and H-phases requires a full local transport analysis, as reported in later sections of the paper.

The confinement properties in the edge which might allow such energy pedestals are not discussed in this paper. None-the-less, it is worth noting that the experimentally determined pressure gradients, though large ($150 kPa.m^{-1}$), lie somewhat below the critical values for the threshold for ballooning instabilities, which have been calculated on the basis of JET H-mode equilibria and a finite aspect ratio ballooning formalism (O 'Brien *et al.*, 1989). However, the experimental values may have been underestimated due to the limited spatial resolution of the LIDAR diagnostic (0.08m). Furthermore, close to the separatrix, coalescence of the first and second stable regions occurs since the total current density (resistive, beam-driven and bootstrap) exceeds the calculated critical value. The dominant contribution to the current density in the edge of an H-mode plasma is the bootstrap current which arises from the steep edge density gradient (Cordey *et al.*, 1988; Stubberfield *et al.*, 1989).

LOCAL TRANSPORT ANALYSIS

The experimental data input to the interpretive codes (TRANSP and FALCON) comprise the time dependence of the magnetic flux surface geometry and the plasma current, the electron density profile (inverted data from a six channel FIR interferometer and LIDAR data when available), the electron temperature profile (ECE data and LIDAR data when available), the ion temperature profile (charge exchange spectroscopy (CXS) of fully stripped carbon and oxygen when available (von Hellermann *et al.*, 1989)), the radiated power profile (inverted bolometer data), the Z_{eff} profile (visible bremsstrahlung, checked against CXS and neutron yield estimates of the deuterium to electron density ratio) and the edge particle confinement time (D_α monitors).

The CXS measurement of the ion temperature profile is not available for the pellet-fuelled ICRF-heated discharge considered here. The profile has been modelled, therefore, with an ion thermal diffusivity, χ_i, proportional to the electron thermal diffusivity, χ_e, the constant of proportionality, $\alpha(t)$, being adjusted in time so that the calculated central ion temperature, $T_i(0)$, matches that obtained from doppler broadening of the He-like nickel line observed with an X-ray crystal spectrometer.

Neutral beam heating and fuelling is calculated using either monte carlo (Goldston *et al.*, 1981) or multiple pencil beam methods (Cordey, Keilhacker and Watkins, 1987). Ion cyclotron resonance heating is calcuated using either a 3-D poloidal mode expansion code (Smithe *et al.*, 1987) or a ray tracing code (Bhatnagar *et al.*, 1984).

The predictive code (JETTO) uses much of the above experimental data as input, except that the electron and ion temperatures are calculated with a model based on the critical temperature gradient model of Rebut, Lallia and Watkins (1989) and then compared with the experimental data.

Local transport analyses use the energy and particle conservation equations (Hawryluk, 1980) to provide, in the first instance, the total heat flux through magnetic surfaces in the interior of the plasma.

An "effective" thermal diffusivity may be defined, such as that obtained from power balance, $\chi_{eff} = Q/n_e \nabla kT_e S$ (where the total heat flux, Q, including the contributions from energy equipartition and convection, across a surface of area, S, is assumed to be proportional to $n_e \nabla kT_e$). In principle, it is possible to proceed further, separating the convective energy losses and, if ion temperature profile data is available, separating the electron and ion conductive energy losses and defining "effective" heat diffusivities, χ_e, and χ_i:

$$q_e = -n_e \chi_e \nabla kT_e \; ; \qquad q_i = -n_i \chi_i \nabla kT_i \tag{4}$$

The "effective" diffusivities shown in this paper are from TRANSP. Similar results are obtained with FALCON and JETTO. Flux surfaces are labelled with either a normalised coordinate, ρ ($0 < \rho < 1$) or the equivalent circular radius, r ($0 < r(m) < 1.5$). The range of interest is usually limited to $0.25 < r(m) < 1.0$. Outside this range the errors become substantial.

The data used for the analyses in this paper are consistent in the sense that the calculated total stored energy, surface voltage (including the contributions from the resistive, beam-driven and bootstrap currents) and total neutron yield (including the contributions from beam-beam, beam-plasma and plasma-plasma reactions) are within the experimental uncertainties on the measurements. None-the less, varying the experimental data within their individual levels of accuracy can introduce a large uncertainty in, for example, the equipartition of energy between electrons and ions and hence in χ_e and χ_i. The errors on χ_e and χ_i are presently estimated at $\pm 50\%$, except when χ_e is apparently much lower than χ_i and the error on χ_e can increase to a factor of 2-3.

MEDIUM DENSITY H-MODE DISCHARGE

The time behaviour of various parameters in the single null X-point JET discharge #15894 is shown in Fig. 5. The L-phase, which lasts for ~0.7s from the start of 8MW of NBI at a time of 14s, is followed by a transition to the H-phase (as indicated by the abrupt fall in the intensity of the D_α emission and the subsequent low level activity). The plasma density, the total stored energy and the neutron reaction rate increase until the H-phase terminates as the NBI power is reduced at 17s. $T_e(0)$ remains roughly constant, or even falls slightly, in time.

The radial profiles of n_e, T_e and T_i are shown in Fig. 4 at a time of 16s, well into the H-phase. In the bulk of the plasma the most characteristic feature is the flat density profile, which changes little as the density increases. The electron temperature also changes little with time. Within the accuracy of the measurements the electron and ion temperatures are the same.

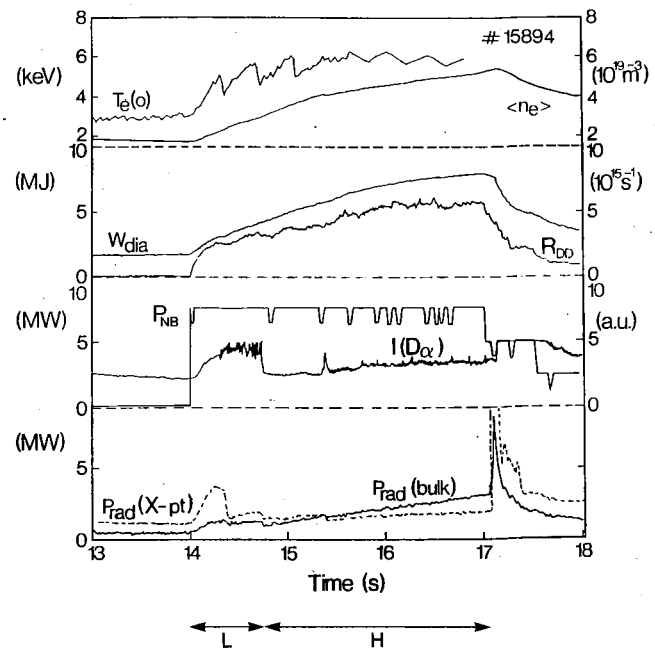

Fig. 5. Time behaviour of electron temperature on axis, $T_e(0)$, volume averaged electron density, $<ne>$, total stored energy, W, neutron reaction rate, R_{DD}, neutral beam power, P_{NB}, D_α intensity, $I(D_\alpha)$, bulk radiation, P_{rad}(bulk) and X-point radiation, P_{rad}(X-pt) for a 3MA/3.1T JET single null X-point discharge.

During the L-phase of the discharge the neutral beam deposition profile is reasonably peaked. The ion power balance is between NBI and ion thermal conduction. In the electron power balance similar levels of NBI and ohmic power are lost mainly by electron heat conduction. The stored energy increases throughout the L-phase, largely due to the increasing density from beam fuelling and recycling. The higher densities achieved during the H-phase of the discharge lead to poor penetration of the NBI with deposition profiles becoming peaked outwardly. Energy equipartition can increase in importance, particularly in the outer regions shown but, since the electron and ion temperatures are the same, within their errors, this is a source of considerable uncertainty, particularly in the electron power balance.

The "effective" thermal diffusivity, χ_{eff}, increases to above its ohmic level at the start of neutral beam heating (Keilhacker and the JET Team,1988). It then decreases progressively throughout the L- and H-phases. There is no obvious abrupt change in χ_{eff} at the transition. The present analysis, using the measured ion temperature profiles, indicates that this behaviour in time is reflected by the ion heat conductivity, χ_i (Fig. 6). There is apparently little change in the electron heat conductivity, χ_e, but these low values ($< 1 m^2 s^{-1}$) are subject to large uncertainties from energy equipartition.

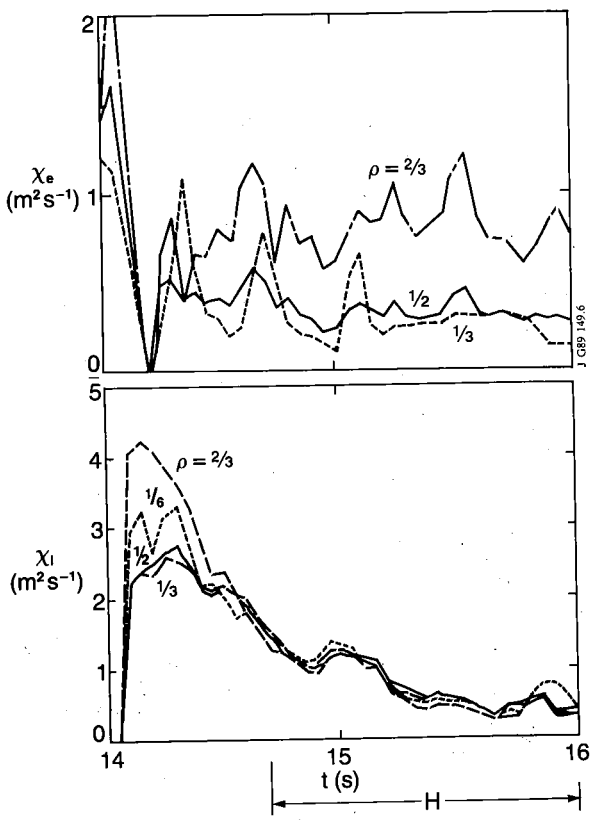

Fig. 6. Time behaviour of the effective heat diffusivities for electrons, χ_e, and ions, χ_i, for JET pulse 15894.

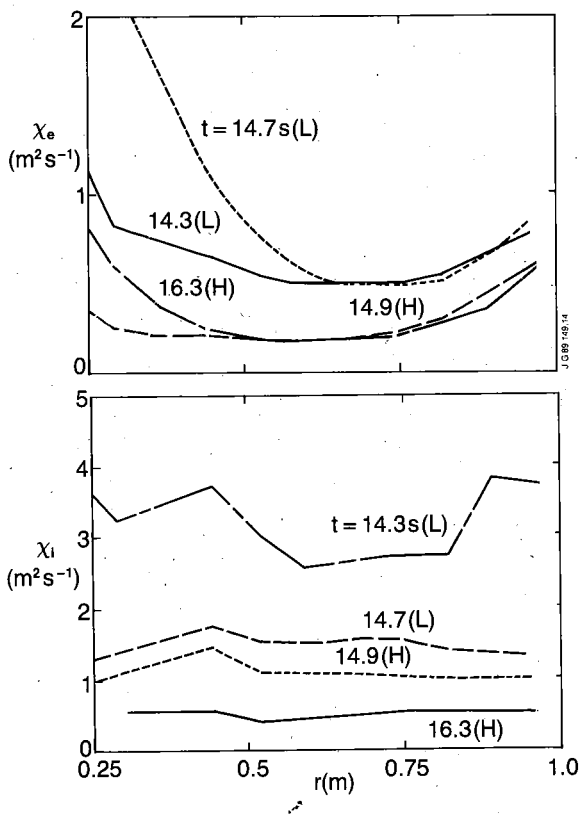

Fig. 7. Spatial profiles of the effective heat diffusivities for electrons, χ_e, and ions, χ_i, for JET pulse 15894.

The spatial profiles of χ_e and χ_i at selected times throughout the discharge (Fig. 7) are rather flat over much of the region shown; further out, the formation of an energy pedestal and losses associated with particle recycling and convection dominate the H-phase. It is to be noted that although χ_i is initially larger than χ_e, χ_i becomes comparable to χ_e, and within 2-3 × $\chi_{i,neo}$, by the end of the H-phase.

HIGH DENSITY PELLET-FUELLED, ICRF-HEATED DISCHARGE

The time behaviour of various parameters of pellet-fuelled, ICRF heated JET discharge #16211 is shown in Fig. 8. A 4mm diameter deuterium pellet is injected at a time of 3s with a multipellet injector developed jointly by ORNL and JET (Kupschus *et al.*, 1987; Milora *et al.*, 1987). The pellet penetrates deep into a deuterium ohmic plasma, reducing T_e and T_i considerably. With up to 8MW of

ICRH both T_e and T_i recover to well in excess of their ohmic values during a phase of "enhanced" confinement and high deuterium neutron yields ($> 10^{15}$n/s).

During this phase the overall energy confinement is some 20% better than after, but the highly peaked density and temperature profiles suggest considerably improved central confinement. At a time of 4.8s there is an abrupt collapse of the central temperatures, density and neutron yield and the overall confinement is reduced.

The different ICRF models tend to agree that heating occurs, predominantly within 0.35m of the magnetic axis and with up to 50% of the input power heating the ions (Bhatnagar *et al.*, 1989; Hammett *et al.*, 1989). On the basis of these results the present transport calculations assume for the ICRF heating a gaussian deposition profile, centred on the magnetic axis and with 50% of the total power heating the electrons and 50% the ions.

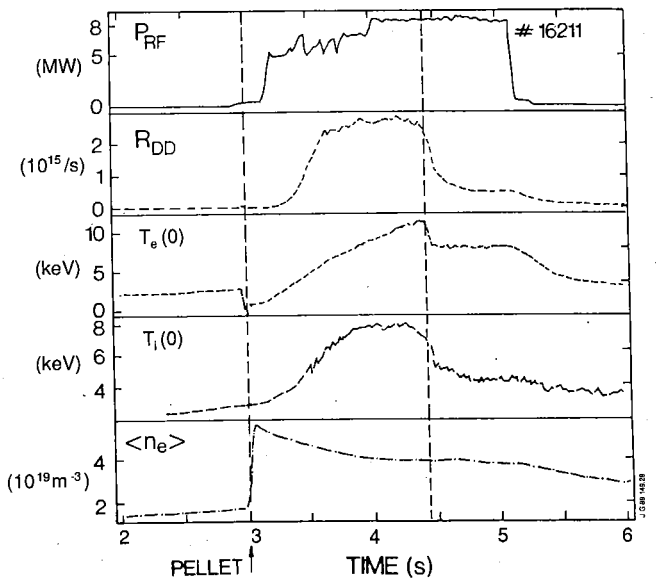

Fig. 8. Time behaviour of ICRF power, P_{RF}, neutron reaction rate, R_{DD}, central electron temperature, $T_e(0)$, central ion temperature, $T_i(0)$ and volume averaged electron density, $< n_e >$ for JET pulse 16211.

During the enhanced confinement phase, at a time of 4.1s, the ion power balance is between ICRF and ion heat conduction. In the electron power balance, the ICRF power to the electrons is comparable to electron heat conduction and the lower ohmic power is comparable to the total radiated power. Following the enhanced confinement phase, at a time of 4.75s, the power balances are somewhat more complicated with energy equipartition contributing some 25% extra (less) power to the ions (electrons), which is taken up by additional (lower) ion (electron) heat conduction losses.

The behaviour of χ_e and χ_i with time at a radius of 0.35m, in the central core of the plasma, is shown in Fig. 9. During much of the enhanced confinement phase (prior to the 'Event') χ_e and χ_i are comparable and low ($< 1 m^2 s^{-1}$). Following this phase both χ_i and χ_e increase by more than a factor of two.

The spatial profiles of χ_e and χ_i at different times throughout the discharge are similar (Fig. 10). During the enhanced confinement phase (4.1s and 4.35s) χ_e and χ_i are significantly lower in the central region than further out. The central values are comparable to $\chi_{i,neo}$. Following this phase, at the later time of 4.75s, the central values of χ_i and χ_e have increased to levels at least comparable to those further out, which have not changed significantly from 4.1-4.75s.

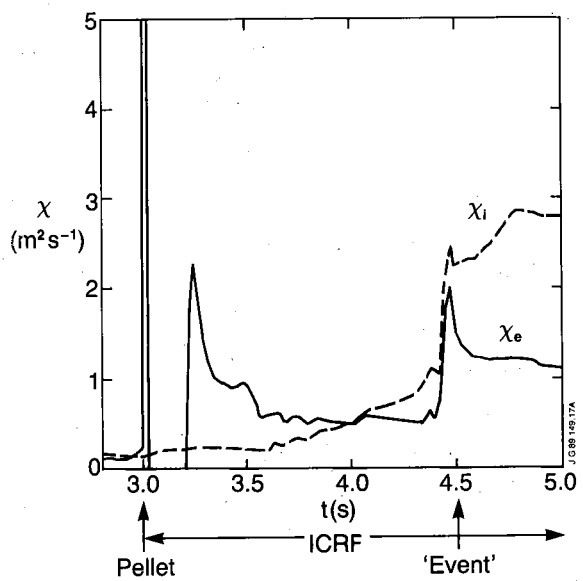

Fig .9. Time behaviour of the effective heat diffusivities for ions, χ_i, and electrons, χ_e, for JET pulse 16211.

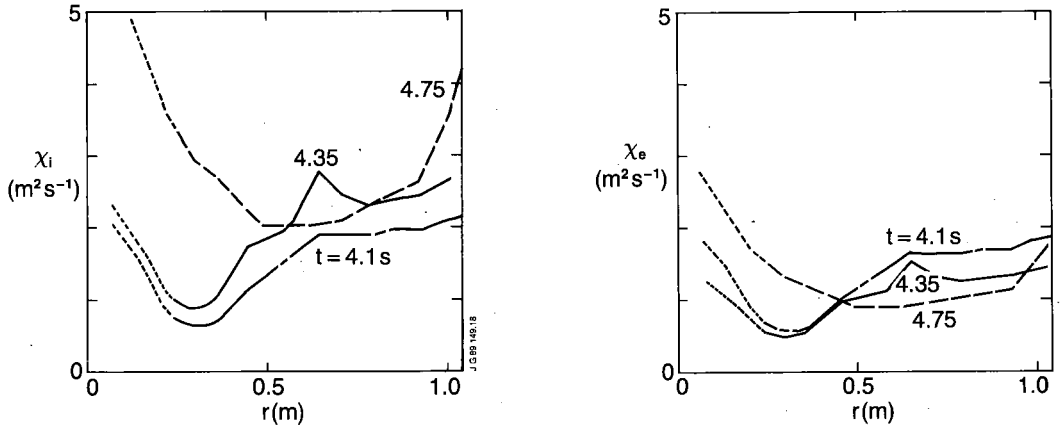

Fig. 10. Spatial profiles of the effective heat diffusivities for ions, χ_i, and electrons, χ_e, for JET pulse 16211.

LOW DENSITY HOT ION MODE

The time behaviour of various parameters in the double null X-point JET discharge #18768 is shown in Fig. 11. The increase in density following up to 21MW of NBI is limited by extensive ^{3}He discharge cleaning prior to operation in deuterium. As a result the NBI profile is very peaked. Heating is predominantly to the ions, with $T_i(0)$, obtained from a fast sampling central channel of the CXS diagnostic, increasing to more than 18keV after 0.5s of heating. $T_e(0) \sim 9$keV is considerably lower. The deuterium neutron yield ($> 10^{16}$n/s) also reaches a maximum at this time, prior to a large influx of carbon (Lowry *et al.*, 1989).

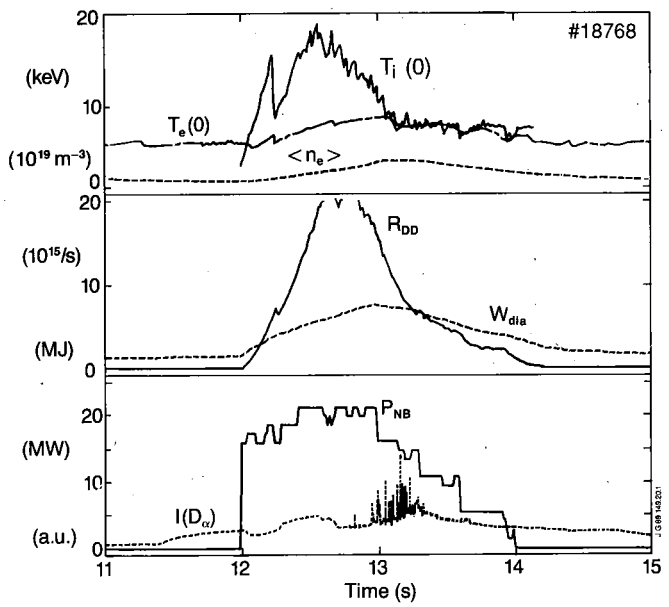

Fig. 11. Time behaviour of central electron temperature, $T_e(0)$, central ion temperature, $T_i(0)$, volume averaged electron density, $< n_e >$, total stored energy, W_{dia}, neutron reaction rate, R_{DD}, neutral beam power, P_{NB} and D_α intensity, $I(D_\alpha)$, for JET pulse 18768.

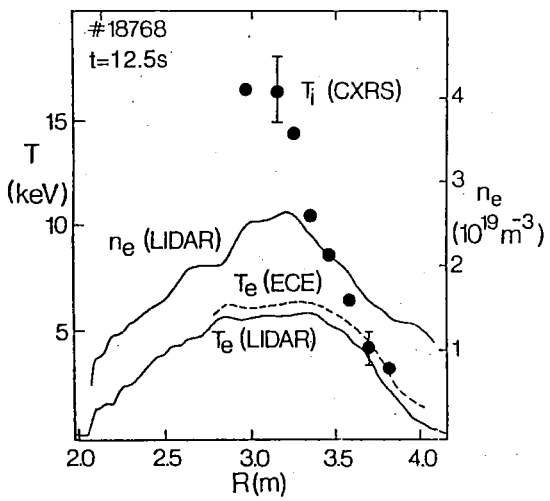

Fig. 12. Radial profiles of electron density, n_e, electron temperature, T_e, and ion temperature, T_i, during the hot ion phase of JET pulse 18768.

The radial profiles of n_e, T_e and T_i are shown in Fig. 12 at the time of maximum neutron yield. The most characteristic feature are the extremely peaked ion temperature profiles and the well peaked density profiles. The electron temperature, determined by both the ECE and LIDAR measurements

is considerably lower than the ion temperature in the central region, but in the outer regions the electron and ion temperatures are the same, to within their error bars.

Over most of the radius the ion power balance is largely between NBI and ion heat conduction. Convective energy losses begin to contribute in the central region. The electron power balance is rather more complicated, with energy equipartition and ohmic heating becoming important, but still less than NBI. In the central region the power loss is shared, approximately equally, by electron heat conduction and convection. In the outer region, the power loss is mainly through radiation and electron heat conduction. The plasma energy is increasing rapidly.

The behaviour of χ_i with time at various radii is shown in Fig. 13 to change little for 1s after NBI begins. The spatial profile of χ_i at a time of 12.5s shows an increase from low central values ($\sim 1 m^2 s^{-1}$, within a factor 2-3 $\times \chi_{i,neo}$) to high values ($\sim 10 m^2 s^{-1}$) in the outer region (Fig. 14). χ_e is low and comparable to the central value of χ_i, but is, however, subject to large uncertainty.

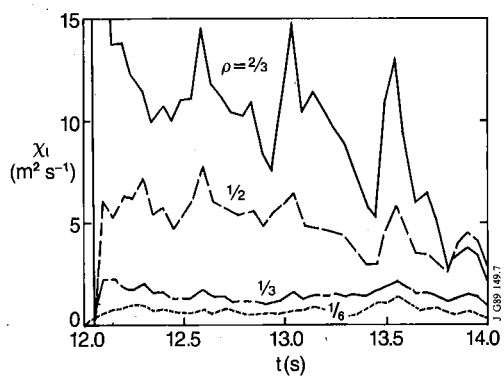

Fig. 13. Time behaviour of the effective ion heat diffusivity, χ_i, for JET pulse 18768.

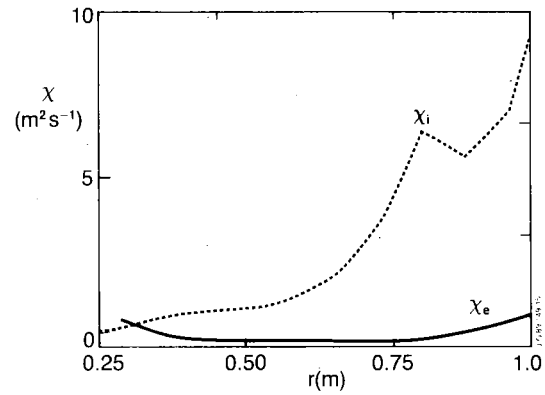

Fig. 14. Spatial profiles of the effective heat diffusivities for ions, χ_i, and electrons, χ_e, for JET pulse 18768.

LOW DENSITY H-MODE DISCHARGE

The time behaviour of various parameters in the double-null X-point JET discharge #18757 is shown in Fig. 15. The increase in density following 10.5MW of NBI is again limited by extensive ^{3}He discharge cleaning prior to operation in deuterium. The NBI profile is very peaked. Heating is predominantly to the ions with $T_i(0)$ increasing to more than 15keV after 0.7s of heating. $T_e(0) \sim 6$keV is considerably lower. The deuterium neutron yield reaches a maximum ($\sim 5 10^{15}$n/s) at this time. Shortly after, following the collapse of a sawtooth, this hot ion plasma makes a transition at constant power to an H-phase (as indicated by the abrupt changes in both the intensity of the D_α emission and the slope of the W_{dia} measurement). During this phase the plasma density and energy increase, $T_i(0)$ decreases and the neutron yield falls slightly.

The radial profiles of n_e, T_e and T_i are shown in Fig. 16, during the hot-ion phase of the discharge. The most characteristic features are the extremely peaked ion temperature and electron density profiles. The electron temperature, determined by both the ECE and LIDAR measurements is considerably lower than the ion temperature in the central region, but in the outer regions the electron and ion temperatures are the same, to within their error bars. Following the transition to the H-phase the density profile, determined from the interferometer data, broadens.

As in the case of the low density hot-ion discharge, in this phase of the present discharge the ion power balance is between NBI and ion thermal conduction. Near the very centre of the plasma, convection is as important as conduction. The electron power balance is again more complicated: convective energy losses are dominant in the central plasma, and comparable to both conduction and radiation further out. The plasma energy increases throughout this phase. During the H-phase of the discharge,

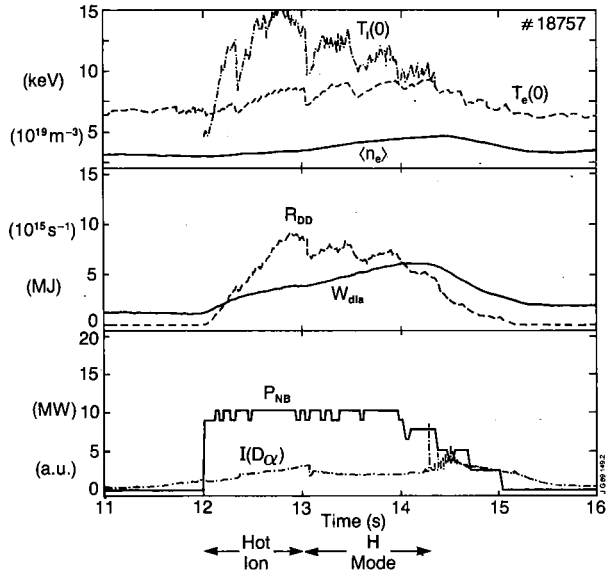

Fig. 15. Time behaviour of central electron temperature, $T_e(0)$, central ion temperature, $T_i(0)$, volume averaged electron density, $< n_e >$, total stored energy, W_{dia}, neutron reaction rate, R_{DD}, neutral beam power, P_{NB} and D_α intensity, $I(D_\alpha)$, for JET pulse 18757.

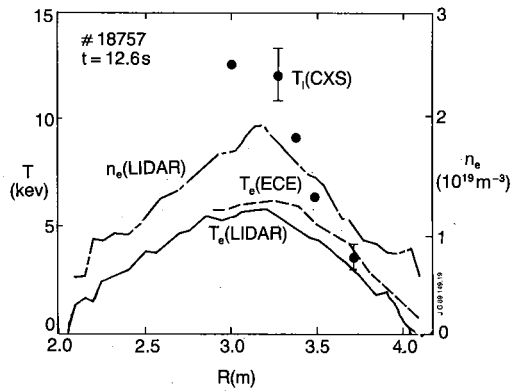

Fig. 16. Radial profiles of electron density, n_e, electron temperature, T_e, and ion temperature, T_i, during the hot ion phase of JET pulse 18757.

conduction remains the dominant loss in the ion power balance. In the electron power balance conduction and radiation remain comparable, but convective energy losses are reduced as a result of the flatter density profiles that develop.

The behaviour of χ_i with time at various radii shows a progressive decrease in the outer region of the discharge, but little change in the centre of the discharge (Fig. 17). As for the medium/high density H-mode discharge there is again no obvious abrupt change in χ_i at the transition from the L-phase to the H-phase at the time of 13s. The spatial profiles of χ_i (Fig. 18) also show low central values, within 2-3 × $\chi_{i,neo}$, and the initially very high value of χ_i in the outer region is reduced in time. Apparently low values of χ_e ($< 1 m^2 s^{-1}$) are obtained, but, again, these are subject to large uncertainty.

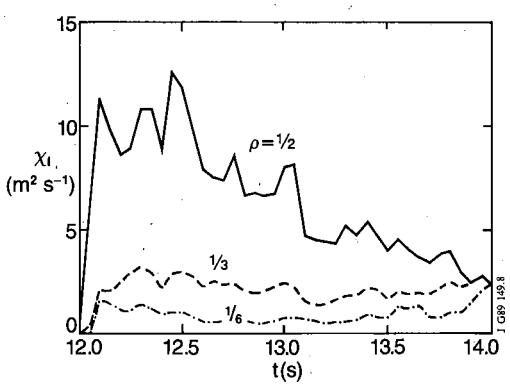

Fig. 17. Time behaviour of the effective ion heat diffusivity, χ_I, for JET pulse 18757.

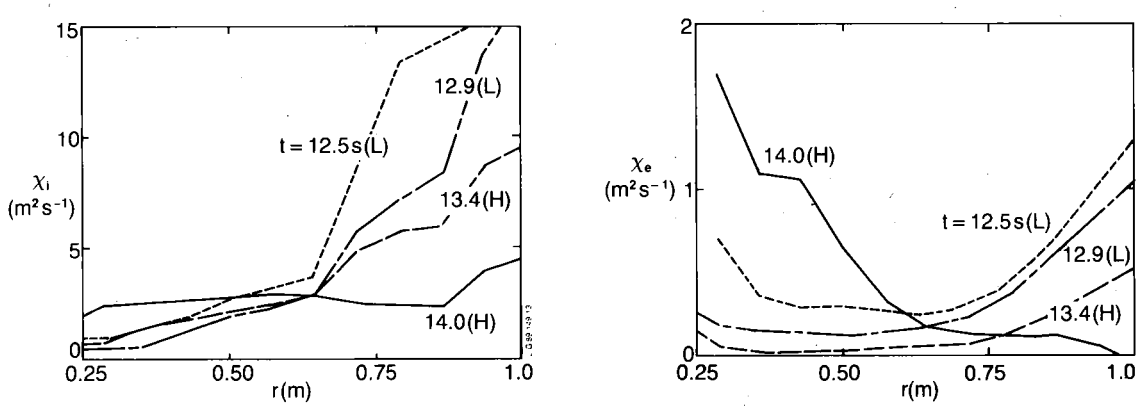

Fig. 18. Spatial profiles of the effective heat diffusivities for ions, χ_I, and electrons, χ_e, for JET pulse 18757.

SUMMARY

The wide variety of diagnostic and analysis facilities available at JET has allowed a study of the confinement properties of plasmas with substantially different temperature and density profiles.

The overall confinement of plasma energy for limiter (L-mode) discharges heated with NBI or ICRF or both is very similar and insensitive to variations by a factor of two in the central temperature and density when the effects of fast particles are taken into account. When strongly peaked density profiles are heated with ICRF the overall confinement is somewhat better (~20%). On the other hand, the overall confinement during the H-phases of X-point discharges is substantially better (×2) than during the preceding L-phases. However, when the contribution of an energy pedestal is taken into account the confinement of the bulk plasma in L- and H-phases is similar. The importance of bootstrap currents and their effect on the stability of ballooning modes when such energy pedestals form is noted.

Local transport analyses, using interpretive and predictive codes and sets of consistent experimental data, provide a better description of confinement. Such analyses have been reported for: a single null X-point medium density, NBI heated H-mode discharge; a limiter, high density, pellet-fuelled and ICRF heated discharge; a double null X-point, low density, NBI heated hot ion discharge; and a double null X-point, low density, high temperature, NBI heated H-mode discharge.

The confinement is described in terms of "effective" heat diffusivities, χ_i and χ_e, having already subtracted convective energy losses which are important only in the extreme hot ion regime and then only near the plasma centre. χ_i can be significantly larger than χ_e for these discharges, in which the ions receive more than 50% of the input power. With peaked density profiles (due to either pellet injection and ICRF heating or NBI heating at low density), the central values of χ_i and χ_e are low (~ $1m^2s^{-1}$, or less). Further out χ_i increases to ~ $2m^2s^{-1}$,or more. In H-mode discharges, χ_i decreases and flattens progressively, as the density increases and broadens with time, ultimately becoming low (~ $1m^2s^{-1}$). There is no obvious abrupt change at the transition from the L-phase to the H-phase. In all cases, the lowest values of χ_i are within a factor of 2-3 $\times\chi_{i,neo}$.

The "effective" diffusivities might appear meaningful for comparison with theory. However, it should be stressed that a specific, purely diffusive, form for the heat flux has been assumed: no attempt has been made, for example, to extract a heat pinch, or similar term, or to separate contributions from different ion species. Furthermore, errors in the experimental data can introduce large uncertainties, particularly in χ_e. None-the-less, low values of χ_e (~ $1m^2s^{-1}$, or less) could be reconciled with heat pulse propagation measurements (χ_{HPP} ~ $3m^2s^{-1}$, Lomas and the JET Team, 1989) through a heat pinch and since χ_i decreases with increasing density, particle and ion heat transport might be related.

REFERENCES

Balet, B. et al. (1989). High Temperature L- and H-mode Confinement in JET. To be submitted to Nuclear Fusion.

Bhatnagar, V. P. et al. (1984). Ray Tracing Modelling of the ICRF Heating of Large Tokamaks. Nuclear Fus., **24**, 955.

Bhatnagar, V. P. et al. (1989). ICRF Power-Deposition Profiles and Heating in Monster Sawtooth and Peaked Density Profile Discharges in JET. *Proc. 16th Eur. Conf. on Cont. Fusion and Plasma Physics, Venice, 1989,* **13B(I)**, 127, EPS.

Bickerton, R. J. and the JET Team. (1989). Latest JET Results and Future Prospects. In: *Plasma Physics and Controlled Fusion Research* (Proc. 12th Int. Conf., Nice, 1988), Paper IAEA-CN-50/A-1-3, IAEA, Vienna.

Callen, J. D. et al. (1987). Modelling of Temperature Profiles and Transport Scaling in Auxiliary Heated Tokamaks. Nucl. Fusion, **27**, 1857.

Cordey, J. G. Keilhacker, M. and Watkins, M. L. (1987). Prospects for Alpha Particle Heating in JET in the Hot Ion Regime. Physica Scripta, **T16**, 127.

Cordey, J. G. et al. (1988). Bootstrap Current Theory and Experimental Evidence. Plasma Physics and Controlled Fusion, **30**, 1625.
Goldston, R. J. et al. (1981). New Techniques for Calculating Heat and Particle Source Rates due to Neutral Beam Injection in Axisymmetric Tokamaks. J. Comput. Phys., **43**, 61.
Hammett, G. W. et al. (1989). Transport Analysis of Pellet-Enhanced ICRH Plasmas in JET. *Proc. 16th Eur. Conf. on Cont. Fusion and Plasma Physics, Venice, 1989,* **13B(I)**, 131, EPS.
Hawryluk, R. J. (1980). An Empirical Approach to Tokamak Transport. *Proc. Course and Workshop, Varenna, 1979,* 19.
Keilhacker, M. and the JET Team. (1989). The JET H-mode at High Current and Power Levels. In: *Plasma Physics and Controlled Fusion Research* (Proc. 12th Int. Conf., Nice, 1988), Paper IAEA-CN-50/A-III-2, IAEA, Vienna.
Kupschus, P. et al. (1987). The JET Multipellet Injector Launcher-Machine Interface. *Proc. 12th Symp. on Fusion Eng., Monterey, 1987,* **2**, 781, IEEE.
Lomas, P. J. and the JET Team. (1989). An Overview of JET Results. Plasma Physics and Controlled Fusion. This Volume.
Lowry, C. G. et al. (1989). The Hot Ion Mode of Small Bore Plasmas in JET. *Proc. 16th Eur. Conf. on Cont. Fusion and Plasma Physics, Venice, 1989,* **13B(I)**, 87, EPS.
Milora, S. L. et al. (1987). Design of a Repeating Pneumatic Pellet Injector for the Joint European Torus. *Proc. 12th Symp. on Fusion Eng., Monterey, 1987,* **2**, 784, IEEE.
Milora, S. L. et al. (1989). Summary of Energy and Particle Confinement in Pellet-Fuelled, Auxiliary-Heated Discharges on JET. *Proc. 16th Eur. Conf. on Cont. Fusion and Plasma Physics, Venice, 1989,* **13B(I)**, 91, EPS.
O' Brien, D. P. et al. (1989). Ballooning Stability Analysis of JET H-mode Discharges. *Proc. 16th Eur. Conf. on Cont. Fusion and Plasma Physics, Venice, 1989,* **13B(I)**, 229, EPS.
Rebut, P. H., Lallia, P. P. and Watkins, M. L. (1989). The Critical Temperature Gradient Model of Plasma Transport: Applications to JET and Future Tokamaks. In: *Plasma Physics and Controlled Fusion Research* (Proc. 12th Int. Conf., Nice, 1988), Paper IAEA-CN-50/D-4-1, IAEA, Vienna.
Schmidt, G. L. and the JET Team. (1989). Heating of Peaked Density Profiles Produced by Pellet Injection in JET. In: *Plasma Physics and Controlled Fusion Research* (Proc. 12th Int. Conf., Nice, 1988), Paper IAEA-CN-50/A-IV-1, IAEA, Vienna.
Smithe, D. N. et al. (1987). An Algorithm for the Calculation of Three-dimensional ICRF Fields in Tokamak Geometry. Nuclear Fus., **27**, 1319.
Start, D. F. et al. (1989). Experimental and Theoretical Studies of Ion Cyclotron Heating on JET. In: *Plasma Physics and Controlled Fusion Research* (Proc. 12th Int. Conf., Nice, 1988), Paper IAEA-CN-50/E-II-3, IAEA, Vienna.
Strachan, J. D. et al. (1987). High-temperature Plasmas in the Tokamak Fusion Test Reactor. Phys. Rev. Lett., **58**, 1004.
Stubberfield, P. M. et al. (1989). Current Density Profile Evolution in JET. *Proc. 16th Eur. Conf. on Cont. Fusion and Plasma Physics, Venice, 1989,* **13B(IV)**, 1255, EPS.
Tanga, A. et al. (1987). Experimental Studies in JET with Magnetic Separatrix. In: *Plasma Physics and Controlled Fusion Research 1986* (Proc. 11th Int. Conf., Kyoto, 1986), **1**, 65, IAEA, Vienna.
Taroni, A. et al. (1989). Global Power Balance and Local Heat Transport in JET. In: *Plasma Physics and Controlled Fusion Research* (Proc. 12th Int. Conf., Nice, 1988), Paper IAEA-CN-50/A-7-1, IAEA, Vienna.
Thomas, P. R. and the JET Team. (1989). High Temperature Experiments and Fusion Product Measurements in JET. In: *Plasma Physics and Controlled Fusion Research* (Proc. 12th Int. Conf., Nice, 1988), Paper IAEA-CN-50/A-4-4, IAEA, Vienna.
Thomsen, K. et al. (1989). Offset-linear Description of H-mode Confinement. *Proc. 16th Eur. Conf. on Cont. Fusion and Plasma Physics, Venice, 1989,* **13B(I)**, 233, EPS.
Tibone, F. et al. (1989). Ion Thermal Conductivity and Convective Energy Transport in JET Hot-ion Regimes and H-modes. *Proc. 16th Eur. Conf. on Cont. Fusion and Plasma Physics, Venice, 1989,* **13B(I)**, 283, EPS.
Tubbing, B. et al. (1989). Double Null X-point Operation in JET with NBI and ICRH Heating. *Proc. 16th Eur. Conf. on Cont. Fusion and Plasma Physics, Venice, 1989,* **13B(I)**, 237, EPS.
von Hellermann, M. et al. (1989). Ion Temperature Profiles in JET. *Proc. 16th Eur. Conf. on Cont. Fusion and Plasma Physics, Venice, 1989,* **13B(I)**, 107, EPS.